Langmuir

Article

pubs.acs.org/Langmuir

Poloidal Flow and Toroidal Particle Ring Formation in a Sessile Drop Driven by Megahertz Order Vibration

Amgad R. Rezk, Leslie Y. Yeo, and James R. Friend*

Micro/Nanophysics Research Laboratory, Royal Melbourne Institute of Technology (RMIT) University, Melbourne, Victoria 3000, Australia

ABSTRACT: Poloidal flow is curiously formed in a microliter sessile water drop over 157−225 MHz because of acoustic streaming from three-dimensional standing Lamb waves in a lithium niobate substrate. The flow possesses radial symmetry with downwelling at the center and upwelling around the periphery of the drop. Outside this frequency range, the attenuation occurs over a length scale incompatible with the drop size and the poloidal flow vanishes. Remarkably, shear-induced migration was found to drive toroidal particle ring formation with diameters inversely proportional to the frequency of the acoustic irradiation.

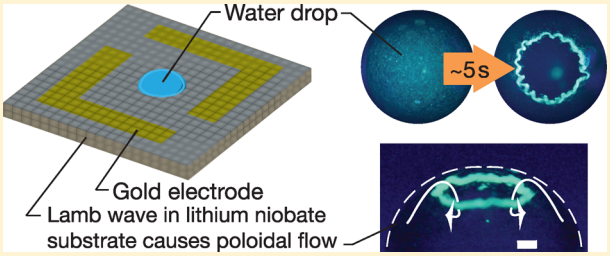

INTRODUCTION

The manipulation of fluids by high-frequency, 1−1000 MHz acoustic waves[1,2] has recently produced many spectacular phenomena, from fluid jetting,[3] dynamic spreading, and fingering instabilities[4] to chaotic advection.[5] We report the appearance of poloidal flow in a sessile drop via high-frequency acoustic excitation, recirculation about a circular locus with a characteristic length scale defined by the confinement of the fluid, because it is in toroidal tokamaks intended for plasma containment in nuclear fusion,[6] in the mantle between the solid core and flexible crust of the earth,[7] and in immiscible spherical drops[8] within another fluid and transported because of acceleration. In every case, the force or acceleration applied to the fluid has an axis of symmetry perpendicular to and in the center of the recirculation trajectory. Such flows have not been observed in microscale sessile drops, let alone in one excited by vibration: acoustic waves have been known to generate azimuthal recirculation in fluids but never to form poloidal flows, as shown in Figure 1.

Rarely used, Lamb wave vibration is actually vital in generating this flow phenomena, a surprising outcome given its standing wave and lossy characteristics, with the perception of being equally or more challenging to form than other waveforms, and the overwhelming emphasis in the discipline on Rayleigh surface wave excitation. Rayleigh surface acoustic waves are prevalent in high-frequency acoustic microfluidic manipulation, with other forms of vibration very rare by comparison at any frequency: thickness,[9] flexural,[10] and Lamb wave vibration with either piezoelectric thin films[11] or mode conversion[12,13] are the few examples known to the authors. In these cases, the frequencies used are less than 10 MHz and the fluid flow has been weak (μm/s order), likely the reason for the few associated publications. In contrast, the higher order, 100 MHz order Lamb waves generated here have not yet been observed to drive fluid flows, let alone flows sufficient to cause the unique phenomena reported in this study. Further, we show that the vibration can be effectively driven using very simple electrode structures (Figure 1a), eliminating the elaborate fabrication typical of acoustic microfluidic devices.

DEVICE FABRICATION AND EXPERIMENTAL PROCEDURE

The Lamb wave device in Figures 1a and 2a was fabricated using a liftoff technique with polyimide tape (Kapton, DuPont, Wilmington, DE) and the sputtering of 150 nm gold. Our choice of L-shaped electrodes forms fully three-dimensional standing Lamb waves, with resonance frequencies defined by the 500 μm thickness of the lithium niobate (LN, 127.86° Y-rotated, X-propagating cut, Roditi, U.K.) substrate:[14] the fundamental Lamb wave mode appears at 3.5 MHz, possessing a wavelength of 1 mm, and harmonics consistently appear at 7 MHz increments to beyond 250 MHz. These details and the absence of other, spurious waves were verified by measuring the spatial distribution of the transverse (z-axis oriented) vibration velocity U across the LN surface with a scanning laser Doppler vibrometer (LDV, UHF-120, Polytec GmBH, Waldbronn, Germany). Perhaps surprisingly, the resonance frequencies only weakly depend upon the electrode geometry and the mounting of the substrate.

For the flow experiments, water drops of radii R = 1.5 mm were placed on the substrate and a signal generator (SML01, Rhode & Schwarz Pty. Ltd., North Ryde, New South Wales, Australia) and amplifier (10W1000C, Amplifier Research, Souderton, PA) were used to provide a continuous sinusoidal electrical input at the defined frequency f. The drop diameter was chosen as an easily reproducible size that provides the broad range of phenomena witnessed in this study. Polystyrene spherical particles $a \approx 5$ μm in diameter (Polysciences, Inc., Warrington, PA) were employed to visually track the flow in the drop; these particles are below the critical size at which direct acoustic forces influence their behavior[15] and, hence, can be assumed to describe the characteristics of the flow via Stokes drag until they reach a sufficient packing density along the streamline, after which

Received: June 12, 2014
Revised: August 18, 2014
Published: September 3, 2014

ACS Publications © 2014 American Chemical Society

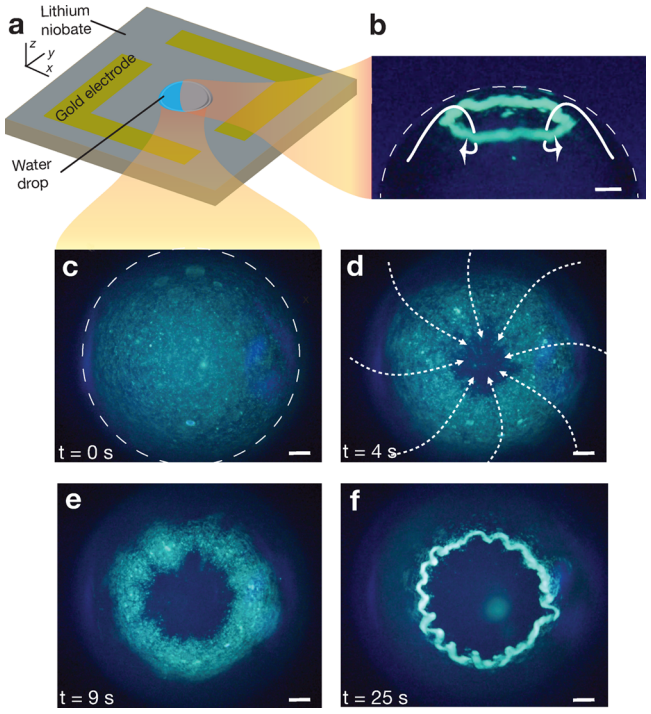

Figure 1. (a) Sessile fluid drop (3 μL) is placed on the 500 μm thick LN substrate with L-shaped Au electrodes from 3.5 to 225 MHz and beyond (not to scale). (b) Side view of the sessile drop with suspended particles undergoing vibration at 225.3 MHz and 0.8 W, showing a particle-laden torus because of the poloidal flow; its formation is illustrated in (c–f) a sequence of top-view images for the same drop. Dotted lines (in panels b and c) indicate the drop edges. Scale bars ~ 300 μm.

independent particle shear diffusion dynamics take over. As shown in a side view in Figure 1b and from the top in panels c–f of Figure 1, the Lamb wave drives poloidal flow in the sessile drop at 225.3 MHz, leading to the formation of a toroidal particle ring via shear migration. To the best of our knowledge, this constitutes the first observation of shear-induced particle migration in the poloidal direction and consequent toroidal particle ring formation.

LAMB WAVE ATTENUATION

Although the substrate vibration assumes a checkerboard standing wave pattern in the absence of the drop (Figure 2b), placement of the drop causes absorption of acoustic energy from the substrate, reducing the standing wave behavior in favor of traveling waves toward and radially symmetric about the drop, behavior that may be characterized by the standing wave ratio, SWR $\equiv \max_\Omega f(\Omega)/\min_\Omega f(\Omega)$, where Ω is some spatiotemporal domain, defined here as one Lamb wavelength λ_{Lamb} along any radial line A–B adjacent to the drop (panels a and c of Figure 2) at a particular instant. The SWR facilitates the computation of the energy loss to input ratio, $\eta \equiv E_{loss}/E_{in} = 4SWR/(SWR^2 + 2SWR + 1)$,[16] where SWR = ∞ for a lossless device and SWR = 1 for a perfectly lossy device. A SWR of 4 from Figure 2c indicates an acoustic energy loss of approximately η = 64% because of mounting of the device in the absence of the drop. With the drop, the energy loss increases to η = 89%. Given that the LN is otherwise nearly lossless, it is reasonable to assume that the increase in energy loss, 25%, is due to the drop absorbing energy and forming sound waves in the fluid, which propagate at the Rayleigh angle, $\theta_R = \sin^{-1}c/c_{Lamb}$, with c being the sound speed in the liquid

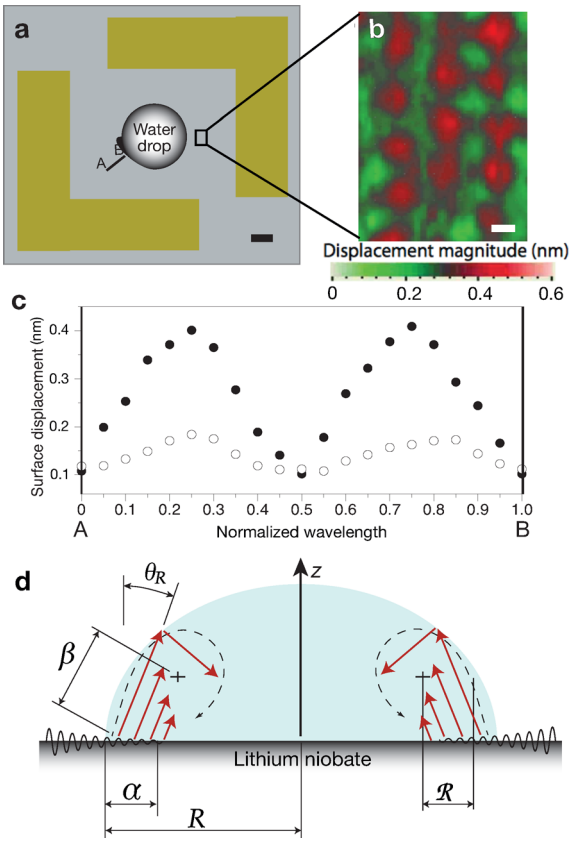

Figure 2. (a) Top view of the LN substrate showing the L-shaped electrodes and the sessile drop (scale bar is 1 mm). The small box represents (b) a LDV scan of the Lamb wave vibration present on the LN surface at a resonant frequency of 157 MHz without the water drop ($\lambda_{Lamb,157\ MHz}$ = 23 μm; scale bar is 10 μm), and A–B represents a radial line over which the LDV was used to measure (c) the transverse displacement of the LN substrate surface, useful for determining the SWR. The SWR decreases from approximately 4 (●) in the absence of the drop to 2 (○) because of (d) the absorption of acoustic energy and attenuation of the Lamb wave of the drop and the formation of a rapidly attenuating sound wave in the drop, each of which occur over specific length scales: α^{-1} and β^{-1} are the attenuation lengths for the Lamb wave in the LN and sound in the fluid, respectively, while $\mathcal{R}$ and R are the recirculation length scale and the drop radius, respectively.

(1482 m/s for water) and c_{Lamb} being the Lamb wave speed. Lamb waves are inherently dispersive, and therefore, both the wave speed and Rayleigh angle are dependent upon the frequency.[17] However, for the high-order harmonics used in this study at 25 MHz and beyond, $c_{Lamb} \rightarrow$ 4000 m/s[17] and, therefore, $\theta_R \approx 22°$.

The Lamb wave itself is attenuated in the solid substrate because of the presence of the drop over a distance α^{-1}, where α is the attenuation coefficient and, for high-order modes, can be approximated as[20]

$$\alpha^{-1} \approx \frac{\rho c}{\rho_{LN} c_{Lamb} \lambda_{Lamb}} \quad (1)$$

where ρ and ρ_{LN} are the liquid (998 kg/m^3) and LN (4630 kg/m^3) densities, respectively. With c_{Lamb} = 4000 m/s, α^{-1} = 2.5, 0.35, and 0.18 mm for Lamb wave resonances at 25, 157, and 225.3 MHz, respectively. Notably, α^{-1} falls below R = 1.5 mm for the higher pair of frequencies: the Lamb wave cannot be sustained along the substrate to the center of the drop, and therefore, any energy leakage into the drop occurs over a region

dx.doi.org/10.1021/la502301f | Langmuir 2014, 30, 11243–11247

α^{-1} radially inward from the edge of the drop. The sound waves in the fluid, however, propagate in the fluid over an attenuation length β^{-1}, where

$$\beta^{-1} = \frac{4\pi^2 f^2}{\rho c^3}\left(\frac{4\mu}{3} + \mu'\right) \quad (2)$$

is generally longer than α^{-1}; β^{-1} = 80, 1.5, and 1 mm for 25, 157, and 225.3 MHz, respectively. μ and μ' are the shear and bulk viscosities. Like the attenuation length in the substrate, α^{-1}, the fluid attenuation β^{-1} also decreases below R for the higher pair of frequencies, implying that the sound is attenuated in the drop before it can reach the center.

POLOIDAL FLOW FORMATION

The attenuation in the substrate and fluid suggests that a central core of the drop with dimension $R - \beta^{-1}$ is not exposed to any acoustic radiation when $\beta^{-1} < R$. To confirm the formation mechanism for the central core, we used a very small drop of diameter $2R$ = 0.5 mm and observed that the poloidal flow cannot be formed at even the highest frequency that we tested (225.3 MHz) because α^{-1} and β^{-1} are large compared to R in this arrangement. Similarly, larger drops of $2R$ = 6 mm show no poloidal flow even at a low excitation frequency of 25 MHz.

We note that, despite the Cartesian form of the Lamb wave in the LN substrate, the radial symmetry of the poloidal flow indicates that the acoustic excitation is symmetric about the z axis from the center of the drop: there are no first-order circumferential variations in the acoustic radiation in the drop, supported by the observation that nearly 90% of the energy of the Lamb wave is lost to the drop and the mounting of the substrate. With acoustic streaming driven by the propagation of the sound in the drop,[21] where it exists about the periphery of the drop, a poloidal flow is formed. The flow has a characteristic recirculation length scale $\mathcal{R}$ that closely corresponds to the length scale of the acoustic attenuation from the drop edge inward, $\mathcal{R} \sim \alpha^{-1}$, as shown in panels b–f of Figure 1 and Figure 3.

NUMERICS

Numerical simulations of the flow that account for the attenuated acoustic wave coupling and the resultant acoustic streaming closely correspond to the experimentally observed flow phenomena. Finite element analysis (ANSYS CFX 14.5, Canonsburg, PA) was used with an 850 000 node brick mesh representing a hemispherical, single-phase water drop with diameter $2R$ = 3 mm, a pinned contact line, and a shear-free boundary for the air–water interface, with a 3 μm node–node separation to properly treat the wave propagation and its attenuation. The pinning and fixed hemispherical shape were justified through the absence of any contact line spreading or drop shape variations in the experiments. The analyses were run until the momentum and mass residuals decreased below 10^{-6}. Laminar flow was assumed in the model because of the low Reynolds number of the flow in the setup and based on past evidence of the laminarity of the acoustic streaming under our experimental conditions.[22] Because the acoustic streaming remains laminar, no capillary waves were expected,[23] as verified using the LDV, and the free surface was safely assumed to be stationary. The fluid–substrate vibration coupling was defined through an effective slip boundary condition at z = 0, incorporating the drift flow generated by the waves[24]

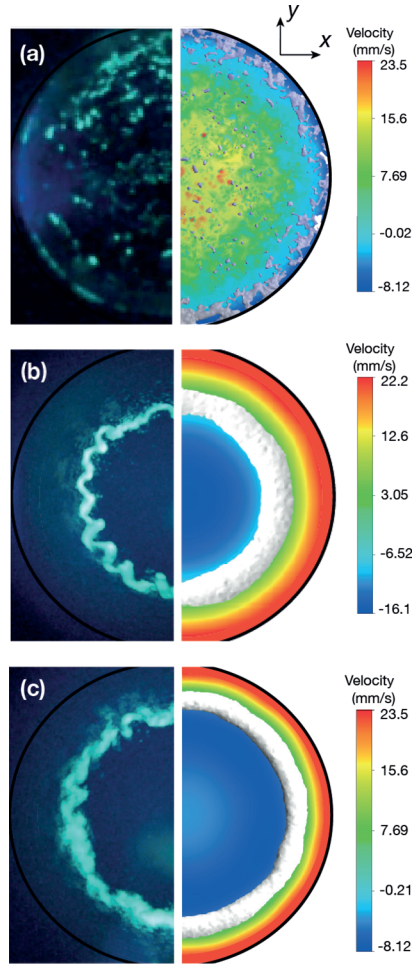

Figure 3. Plane cross-sectional view comparison of the experimental particle behavior in (left) the 3 μL, $2R$ = 3 mm diameter drop and (right) z-axis fluid velocity predictions of the finite element analysis. At (a) 25 MHz, the acoustic streaming is present throughout the drop in both the experiment and analysis, and instead of poloidal flow, bulk recirculation reminiscent of many acoustic drop manipulation experiments is present,[18] leading to the dispersion of the particles.[19] At (b) 157 MHz, however, poloidal flow occurs and a toroidal particle ring is formed, corresponding to, in the analysis results, a region possessing vorticity equal to or greater than 0.5 s^{-1}, a simple but effective means to track the circular vortex at the core of the poloidal flow. Increasing the excitation frequency to 225.3 MHz (bottom image) produces a larger particle vortex ring because of the reduced attenuation lengths α^{-1} and β^{-1}, placing the vortex core closer to the edge of the drop.

$$\begin{pmatrix} u_r \\ u_z \end{pmatrix} = \begin{pmatrix} (\varepsilon\chi\xi U/2\eta)e^{-2\alpha(R-r)} \\ \alpha\delta z\varepsilon\chi\xi U(R-r)e^{-2\alpha(R-r)} \end{pmatrix} \quad (3)$$

in which r is the radial coordinate, u_r and u_z are the radial and axial drift velocities, respectively, $\varepsilon \equiv U/c$ is the acoustic Mach number, $\chi \approx 1$ is the ratio between the longitudinal and transverse velocity components of the wave, φ is the phase angle between the longitudinal and transverse velocity components of the wave, $\xi \equiv (\cos\phi - \sin\phi)$, and $\delta \equiv (4\pi\mu/\rho f)^{1/2}$ is the characteristic thickness of the viscous boundary layer.

dx.doi.org/10.1021/la502301f | Langmuir 2014, 30, 11243–11247

PARTICLE VORTEX RING FORMATION

The formation of the toroidal particle vortex ring typically exemplified in panels c–f of Figure 1 can be attributed to the homogenization of the suspended particles that are swept by the poloidal flow trajectory into closed streamlines of radius $\mathcal{R}$. Because of the higher velocities along the outer streamlines, a shear gradient exists that, when the local volume fraction of the particles along the streamline ϕ exceeds a critical value (usually corresponding to the maximum packing fraction of 0.68 for hard spheres), results in cross-streamline particle transport from the high shear regions along the outer streamlines[25] to populate the low shear interior regions of the poloidal flow, as illustrated by the schematic in Figure 4. This is verified by the

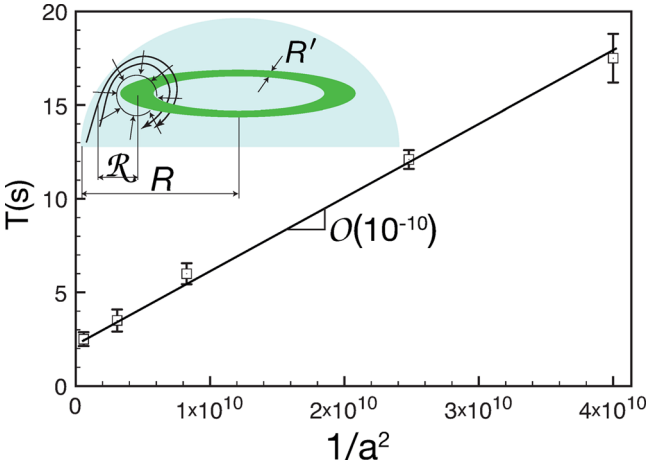

Figure 4. Shear diffusion mechanism responsible for the formation of the toroidal particle vortex ring, because of poloidal flow recirculation, is illustrated in an inset of a plot of the corresponding time for its formation T as a function of the particle size a. The initial particle concentration was 10^5 particles/mL. Here, the input power to the device is held constant at 0.8 W.

time taken for the particles to aggregate into the toroidal ring pattern T, which scales as $1/a^2$, as shown in Figure 4, as might be expected given an effective cross-streamline diffusion rate $\dot{\gamma}\phi a^2$, which translates into a particle diffusion time $T_{sm} \sim R'^2/\dot{\gamma}\phi a^2$, where $\dot{\gamma}$ is the shear rate and R' is the thickness of the particle ring. Moreover, the slope $K \sim R'^2/\dot{\gamma}\phi \sim O(10^{-10})$ with experimental parameters $R' \sim 0.1$ mm, $a \sim 10$ μm, and $\dot{\gamma} \sim V/R' \sim 10^{-3}/10^{-4} \sim 10$ s^{-1}, wherein V is the characteristic velocity scale of the poloidal recirculation, is consistent with Figure 4, equating to particle diffusion times of approximately 10 s. Further, we note the existence of an azimuthally distributed instability in the toroidal particle ring in Figure 3, reminiscent of the well-known vortex ring instability[26] but distinct in that the wavelength of the instability appears to be independent of the poloidal flow speed in the drop.

CONCLUSION

In summary, we report the existence of a poloidal flow arising within a sessile fluid drop vibrated at MHz order frequencies that correspondingly exhibits unique particle aggregation because of shear diffusion into an azimuthal vortical ring with a radius that depends upon the frequency of the underlying acoustic excitation. The poloidal flow is found to exist only above a threshold frequency dependent upon the sessile drop diameter and the attenuation rates of both the acoustic wave in the substrate and in the fluid such that $\alpha/R < 1$ and $\beta/R < 1$.

AUTHOR INFORMATION

Corresponding Author

*E-mail: james.friend@rmit.edu.au.

Notes

The authors declare no competing financial interest.

ACKNOWLEDGMENTS

This work was performed in part at the Melbourne Center for Nanofabrication (MCN) node of the Australian National Fabrication Facility, a company established under the National Collaborative Research Infrastructure Strategy to provide nano- and microfabrication facilities for Australia's researchers. James R. Friend is grateful for support of the work by Australian Research Council Grants DP120100013 and DP120100835. Leslie Y. Yeo is grateful for funding from the Australian Research Council for an Australian Research Fellowship under Discovery Grant Project DP0985253. James R. Friend is grateful to the Melbourne Center for Nanofabrication for a Senior Tech Fellowship and to RMIT University for a Vice-Chancellor's Senior Research Fellowship.

REFERENCES

(1) Friend, J.; Yeo, L. Y. Microscale acoustofluidics: Microfluidics driven via acoustics and ultrasonics. *Rev. Mod. Phys.* **2011**, *83*, 647–704.
(2) Lin, S.-C. S.; Mao, X.; Huang, T. J. Surface acoustic wave (SAW) acoustophoresis: now and beyond. *Lab Chip* **2012**, *12*, 2766–2770.
(3) Tan, M. K.; Friend, J. R.; Yeo, L. Y. Interfacial jetting phenomena induced by focused surface vibrations. *Phys. Rev. Lett.* **2009**, *103*, 024501.
(4) Rezk, A. R.; Manor, O.; Friend, J. R.; Yeo, L. Y. Unique fingering instabilities and soliton-like wave propagation in thin acoustowetting films. *Nat. Commun.* **2012**, *3*, 1167.
(5) Frommelt, T.; Kostur, M.; Wenzel-Schäfer, M.; Talkner, P.; Hänggi, P.; Wixforth, A. Microfluidic mixing via acoustically driven chaotic advection. *Phys. Rev. Lett.* **2008**, *100*, 034502.
(6) Jaeger, E. F.; Berry, L. A.; Myra, J. R.; Batchelor, D. B.; D'Azevedo, E.; Bonoli, P. T.; Phillips, C. K.; Smithe, D. N.; D'Ippolito, D. A.; Carter, M. D.; Dumont, R. J.; Wright, J. C.; Harvey, R. W. Sheared poloidal flow driven by mode conversion in tokamak plasmas. *Phys. Rev. Lett.* **2003**, *90*, 195001.
(7) Forte, A. M.; Peltier, W. R. The kinematics and dynamics of poloidal-toroidal coupling in mantle flow: The importance of surface plates and lateral viscosity variations. *Adv. Geophys.* **1994**, *36*, 1–119.
(8) Bush, J.; Stone, H.; Bloxham, J. Axial drop motion in rotating fluids. *J. Fluid Mech.* **1995**, *282*, 247–278.
(9) Yang, Z.; Matsumoto, S.; Goto, H.; Matsumoto, M.; Maeda, R. Ultrasonic micromixer for microfluidic systems. *Sens. Actuators, A* **2001**, *93*, 266–272.
(10) Meng, A. H.; Nguyen, N.-T.; White, R. M. Focused flow micropump using ultrasonic flexural plate waves. *Biomed. Microdevices* **2000**, *2*, 169–174.
(11) Moroney, R.; White, R.; Howe, R. Microtransport induced by ultrasonic Lamb waves. *Appl. Phys. Lett.* **1991**, *59*, 774.
(12) Hodgson, R. P.; Tan, M.; Yeo, L.; Friend, J. Transmitting high power RF acoustic radiation via fluid couplants into superstrates for microfluidics. *Appl. Phys. Lett.* **2009**, *94*, 024102.
(13) Liang, W.; Lindner, G. Investigations of droplet movement excited by Lamb waves on a non-piezoelectric substrate. *J. Appl. Phys.* **2013**, *114*, 044501.
(14) Viktorov, I. A. *Rayleigh and Lamb Waves: Physical Theory and Applications*; Plenum Press: New York, 1967; Vol. *147*.

(15) Rogers, P. R.; Friend, J. R.; Yeo, L. Y. Exploitation of surface acoustic waves to drive size-dependent microparticle concentration within a droplet. *Lab Chip* **2010**, *10*, 2979−2985.
(16) Jones, M. G.; Stiede, P. E. Comparison of methods for determining specific acoustic impedance. *J. Acoust. Soc. Am.* **1997**, *101*, 2694−2704.
(17) Wu, T.-C.; Wu, T.-T.; Hsu, J.-C. Waveguiding and frequency selection of Lamb waves in a plate with a periodic stubbed surface. *Phys. Rev. B: Condens. Matter Mater. Phys.* **2009**, *79*, 104306.
(18) Brunet, P.; Baudoin, M.; Matar, O. B.; Zoueshtiagh, F. Droplet displacements and oscillations induced by ultrasonic surface acoustic waves: A quantitative study. *Phys. Rev. E: Stat., Nonlinear, Soft Matter Phys.* **2010**, *81*, 036315.
(19) Shilton, R.; Tan, M. K.; Yeo, L. Y.; Friend, J. R. Particle concentration and mixing in microdrops driven by focused surface acoustic waves. *J. Appl. Phys.* **2008**, *104*, 014910−014910.
(20) Cheeke, J. D. N. *Fundamentals and Applications of Ultrasonic Waves*; CRC Press: Boca Raton, FL, 2012.
(21) Eckart, C. Vortices and streams caused by sound waves. *Phys. Rev.* **1948**, *73*, 68−76.
(22) Dentry, M. B.; Yeo, L. Y.; Friend, J. R. Frequency effects on the scale and behavior of acoustic streaming. *Phys. Rev. E: Stat., Nonlinear, Soft Matter Phys.* **2014**, *89*, 013203.
(23) Blamey, J.; Yeo, L. Y.; Friend, J. R. Microscale capillary wave turbulence excited by high frequency vibration. *Langmuir* **2013**, *29*, 3835−3845.
(24) Manor, O.; Yeo, L. Y.; Friend, J. R. The appearance of boundary layers and drift flows due to high-frequency surface waves. *J. Fluid Mech.* **2012**, *707*, 482−495.
(25) Leighton, D.; Acrivos, A. Shear-induced migration of particles in concentrated suspensions. *J. Fluid Mech.* **1987**, *181*, 415−439.
(26) Widnall, S. E.; Bliss, D. B.; Tsai, C.-Y. The instability of short waves on a vortex ring. *J. Fluid Mech.* **1974**, *66*, 35−47.